IEEE Access
Multidisciplinary | Rapid Review | Open Access Journal

Received November 14, 2018, accepted December 2, 2018, date of publication December 17, 2018,
date of current version January 7, 2019.

Digital Object Identifier 10.1109/ACCESS.2018.2886369

The Installation Performance Control of Three Ducts Separate Exhaust Variable Cycle Engine

HAOYING CHEN, HAIBO ZHANG, ZHONGZHI HU, AND QIANGANG ZHENG

Jiangsu Province Key Laboratory of Aerospace Power Systems, College of Energy and Power Engineering, Nanjing University of Aeronautics and Astronautics, Nanjing 210016, China

Corresponding author: Haibo Zhang (zh_zhhb@126.com)

This work was supported by the National Natural Science Foundation of China under Grant 51576096.

ABSTRACT The research on modeling and installation performance control of three ducts separate exhaust variable cycle engine has been studied. In this paper, we established the fan, the low pressure and high pressure compressor model based on the stage-stacking method. On this basis, a component-level mathematical model is constructed and the compressor model of adjustable mode selector valve area, the third bypass and its exhaust nozzle mode are established. Besides, the research took the inlet inside and outside characteristic model into consideration. The simulation showed that the engine could be able to modulate the third bypass airflow adaptively by control of fan vane, mode selector valve area, third bypass, and main exhaust nozzle area. It is possible to continuously match the engine's airflow demand to the inlet's airflow supply. The results show that compared with the mixed exhaust three ducts variable cycle engine, the inlet spillage drag of the separate exhaust variable cycle engine is reduced by about 18%. Under the condition of supersonic flight, the constant flow control can significantly improve the economy of the engine. Compared with the mixed flow variable cycle engine, the inlet spillage drag of the three ducts separate exhaust variable cycle engine is reduced by about 20%.

INDEX TERMS Variable cycle engine, separate exhaust, component-level modeling, spillage drag, the installation performance.

I. INTRODUCTION

With the rapid development of modern aircraft technology, the requirements of propulsion system performance become more severe. The system performance is expected to have higher thrust weight ratio, larger specific thrust, lower specific fuel consumption, higher stability and reliability. In the large envelope range, the conventional aero engine is difficult to take the promotion of power performance and economy into account. And the conventional aero engine can't meet the performance requirements of the modern aircraft. Thus the concept of variable cycle engine(VCE) is proposed [1], [2]. On the one hand, it satisfies the strong military demand, and on the other hand, it meets the needs of supersonic civilian transport aircraft. A large number of effective researches have been carried out on the variable cycle engine. These researches showed that the aerodynamic and thermodynamic cycle of the engine is controlled actively by adjusting the geometry, position and size of the adjustable components under different flight conditions. These adjustments make the engine work close to the optimal cycle parameters. The function of the variable cycle can not only improve the performance of the engine, but also the stable working range of it [3]–[5].

Thus, in the 70s of last century, the United States put forward the supersonic cruise aircraft research program and determined the basic structure of double bypass variable cycle engine GE21 through the General Electric Company(GE). At the beginning of this century, the sixth generation aero-engine design was launched in USA to develop and validate the adaptive engine technology. Significant progress has been made so far and would soon be applied in engineering. The NASA research showed that the variable cycle engine could not only change the engine operating mode timely to meet the needs of different missions, but also significantly improve the coupling between the engine and inlet that would reduce the inlet spillage drag and improve the engine installation thrust. The variable cycle engine has become the focus of military and civil engine research because of its remarkable flow regulation ability, which makes the bypass regulation wider and installation loss smaller. The loss

2169-3536 © 2018 IEEE. Translations and content mining are permitted for academic research only.
Personal use is also permitted, but republication/redistribution requires IEEE permission.
See http://www.ieee.org/publications_standards/publications/rights/index.html for more information.

includes inlet spillage drag and body drag. In 2013, the Air Force Research Laboratory(AFRL) signed contracts with GE and Pratt&Whitney to develop Adaptive Engine Technology Development (AETD). Most of the research is focused on the mixed flow variable cycle engine, the study on unmixed flow variable cycle engine is few and the study of its installation performance is still in blank [7]–[9].

This research is focused on the installation performance control of three ducts separate exhaust variable cycle engine. This engine is different from the structure of F120 and other mixed flow engines, which adds a second independently modulated bypass stream [10]. By modulating airflow to the second and third stream, the engine not only has the multi cycle mode of the conventional variable cycle engine, but also has the ability to keep the flow of the engine constant when the engine is in throttle condition. Thus, the engine significantly reduces the inlet spillage drag and improves the efficiency of the propulsion [11].

During the research, a method of obtaining the characteristics of variable cycle compression components is proposed, which is based on stage-stacking method. Then the component level model of three ducts separate exhaust variable cycle engine is established. And the calculation method of the installation performance is given. In the two typical flight missions of subsonic cruise and supersonic cruise, the changes of spillage drag, net thrust and installation thrust under given control law are studied. Finally, the results of calculation are compared with a mixed type variable cycle engine [12]–[15]. The results shows that the inlet spillage drag of the engine is reduced and the inlet spillage drag decreases more obviously under the constant flow control.

Theoretical research shows that the engine has large thrust loss after the engine is installed on the aircraft. The size of the loss is of great significance to the design of the aircraft and the engine. Because the thrust loss not only affects the design of aircraft shape, but also relates to the choice of engine cycle parameters, inlet and nozzle. Fig.1 shows the change of turbofan thrust, net thrust and the spillage drag under different Mach numbers.

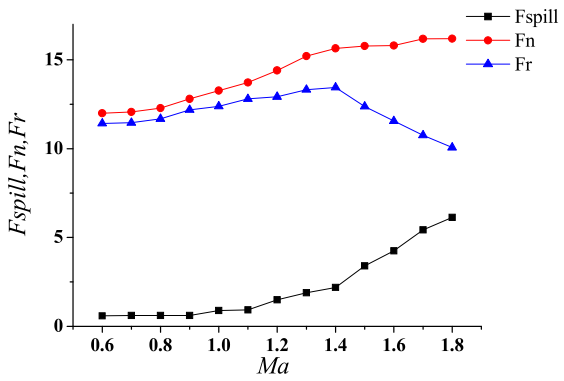

FIGURE 1. Tendency diagram of F_{spill}, F_n, F_r.

Where F_{spill} is the spillage drag, F_n is the thrust, F_r is the net thrust.

It can be seen that when the Mach number is less than 1.2, the inlet spillage drag is small and the influence on the net thrust of the engine is not obvious. When Ma is larger than 1.5, the spillage drag accounts for 30% of the engine thrust. The higher Mach number is, the larger proportion of the drag is. Therefore, the flow control of inlet and engine in supersonic condition should be considered. In other words, the installation performance control of the whole propulsion system ought to be taken into consideration [16].

II. STRUCTURE AND PRINCIPLE OF ANALYSIS

The variable cycle engine could change the bypass ratio by adjusting the flow of bypass stream and primary stream, which makes the engine have good performance in large envelope range. The VCE have drawn wide attention due to its characteristic and the research on double bypass variable cycle engine is particularly popular. Compared with double bypass variable cycle engine, the three ducts variable cycle engine has lower installed drag and higher economy. So it is necessary to study three ducts variable cycle engine. During the research of variable cycle engine, the flow matching problem of engine and inlet is a key part. The flow matching between VCE and inlet is realized by changing the geometry of variable cycle engine, which reduces the spillage drag and improves the thrust performance of engine. Therefore, it is necessary to study the constant flow control of variable cycle engine.

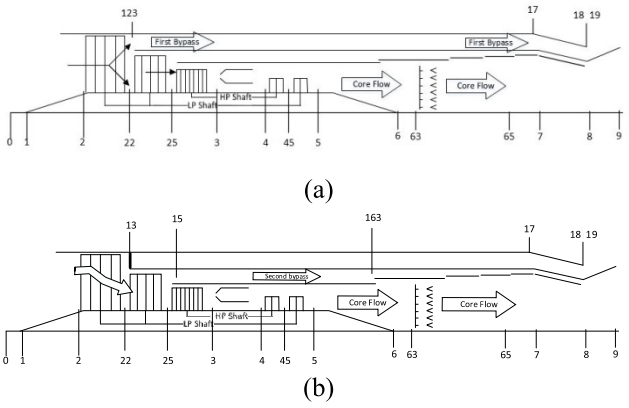

FIGURE 2. Schematic of Variable geometry turbofan engine.

In Figure 2 (a), the schematic diagram of the engine in the three steams mode is given. Compared with the conventional turbofan engine, the engine adds a second independently modulated bypass stream. In Figure 2 (b), the engine closes the mode selection valve and the engine works in the single bypass mode (similar to conventional turbofan engine). The separate exhaust makes the third stream have many functions, which can provide cooling source to cool the heat load of the engine, reduce the heat load of the fuel system and eliminate the problem of fuel coking. Furthermore, it is possible to continuously match the engine's airflow demand to the inlet's airflow supply by modulating airflow to the second and

third streams. The modulation reduces the spillage drag and improve the cycle performance of the engine.

In Fig.2, the section numbers are expressed as, where 1 is the entrance of inlet, 2 is the exit of inlet, 22 is the exit of fan, 25 is the exit of low-pressure compressor(LPC), 3 is the exit of high-pressure compressor(HPC), 4 is the exit of combustor, 45 is the exit of high pressure turbine, 5 is the exit of low pressure turbine, 6 is the mixing chamber, 8 is the exit of nozzle, 123 is the entrance of third steam, 13 is the mode selection valve(MSV), 125 is the entrance of second steam, 18 is the exit of third stream nozzle. All the definitions of bypass ratio are as follows:

$$\begin{aligned} B_{PR1} &= W_{g123}/W_{a22} \\ B_{PR2} &= W_{g15}/W_{a25} \\ OB_{PR} &= (W_{g123} + W_{a15})/W_{a25} \end{aligned} \tag{1}$$

where W_{a25} is the core engine airflow, W_{g15} is the second stream, W_{g123} is the third stream and W_{a2} is the fan's airflow, B_{PR1} represents bypass ratio 1, mass flow of third stream/ mass flow of LPC, B_{PR2} represents bypass ratio 2, mass flow of second stream/ mass flow of HPC, OB_{PR} represents overall bypass ratio, (mass flow in $2^{nd} + 3^{rd}$ streams)/ mass flow of HPC.

The model established in this paper is based on the double bypass variable cycle engine and three ducts adaptive cycle model of General Electric Company. The key components include mode selection valve(MSV), guide vane angle, third stream nozzle area and so on. Through the adjustment of these components, the engine can work steadily and meet the calculation of different operation modes. Then the inlet model is established and the calculation method of inlet/engine installation loss is studied.

III. MATHEMATICAL MODEL

The general compressor components are modeled by the compressor relative rotor speed and pressure ratio. The compressor air flow and efficiency are obtained through the compressor characteristic maps. Then the compressor power, the total temperature and other parameters could be calculated. Therefore, the accurate compressor performance data is essential to the compressor components modeling. On the basis of [17], this paper calculates the characteristic data of fan, low and high pressure compressor through stage-stacking method.

The axial-flow compressor consists of rotor and stator blades. A row of rotor blades and a row of stator blades are generally called the primitive level of the compressor. The axial flow section is shown in Fig.3.

In Fig.3, the upper part is the compressor rotor blade gird and the below is the compressor stator grid. U_c is the circumferential velocity of the compressor blade. C is the absolute velocity of the air. The airflow relative blade velocity is the combined speed of U_c and C. The angle between the absolute velocity and the axial is α. The angle between the relative velocity and the axial is β.

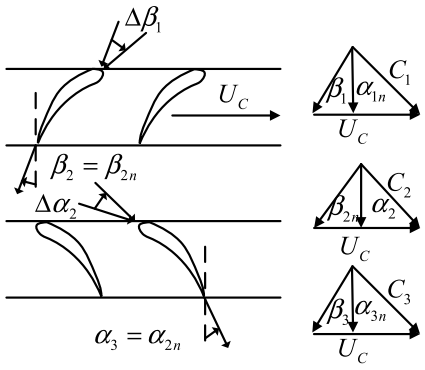

FIGURE 3. Primitive level of compressor.

In each stage of the fan, the rotor blades make work by rotating the gas flow and makes the pressure increase. The stator blade does not work on the air flow, which reduces the air velocity and increases the static pressure of the airflow. The method of calculation can be referred to the literature. Due to the limitation of the article, it would not be repeated here.

When the working state of the fan is not set in the design point state, the blade angle of the inlet airflow would have a deflexion. But the angle of the outflow changes a little. The fan angle of the kth stage can be expressed as:

$$\begin{aligned} \alpha_{1,k} &= \alpha_{3,k-1}\beta_{1,k} = \beta_{1,n} + \Delta\beta_{1,k} \\ \alpha_{2,k} &= \alpha_{2,n} + \Delta\alpha_{2,k}\beta_{2,k} = \beta_{2,n} \\ \alpha_{3,k} &= \alpha_{3,n}\beta_{3,k} = \beta_{3,n} + \Delta\beta_{3,k} \end{aligned} \tag{2}$$

where $\Delta\alpha_{2,k}$, $\Delta\beta_{1,k}$ and $\Delta\beta_{3,k}$ are the flow deflection angles.

The total outlet pressure at kth stage fan rotor blades can be expressed as:

$$P_{02s,k} = P_{01s,k}\left[\eta_{s,k}\left(\frac{T_{02s,k}}{T_{01s,k}} - 1\right) + 1\right]^{\frac{\gamma}{\gamma-1}} \tag{3}$$

where $\eta_{s,k}$ is isentropic efficiency, $\eta_{s,k} = 1 - \varepsilon\left|\Delta\beta_{1,k}/\beta_{1n}\right|$, $P_{01s,k}$, $T_{01s,k}$ are the inlet compressor pressure and temperature of stage k, $P_{02s,k}$, $T_{02s,k}$ are the exit compressor pressure and temperature of stage k rotor. The efficiency is related to the deflection angle of the inlet rotor blade.

$$\Delta\beta_{1,k} = \tan^{-1}\left[\frac{U_C}{C_{a1,k}} - \tan\alpha_{1n}\right] - \beta_{1n} \tag{4}$$

where $C_{a1,k}$ is the axial velocity of stage k compressor blade.

After determining the fan speed and the air flow, the entire pressure ratio and efficiency characteristic maps of the fan could be calculated. As shown in Fig.4. During the calculation of the isentropic compression coefficient, the deflection factor of inlet flow angle(ε) ought to be considered. With the change of the factor values, the calculated fan characteristics have to be changed too. When the positive deflection of guide vane is 0.6, the corresponding fan characteristic curve could be shown in Fig.5.

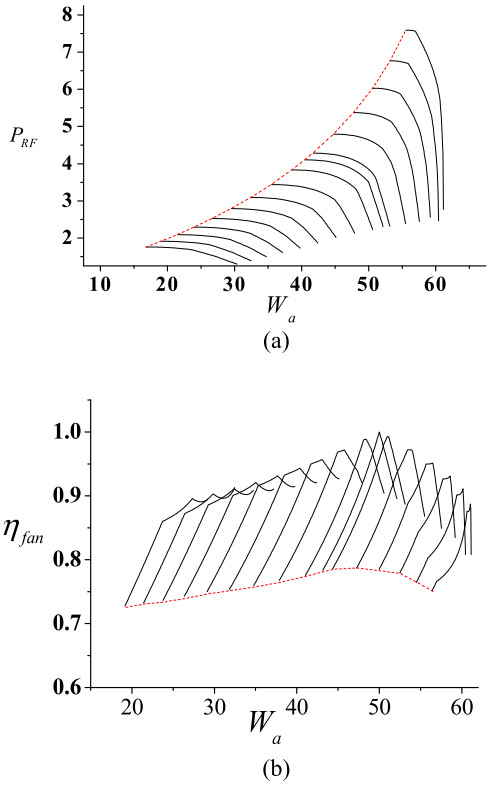

FIGURE 4. Variable geometry component characteristics of fan.

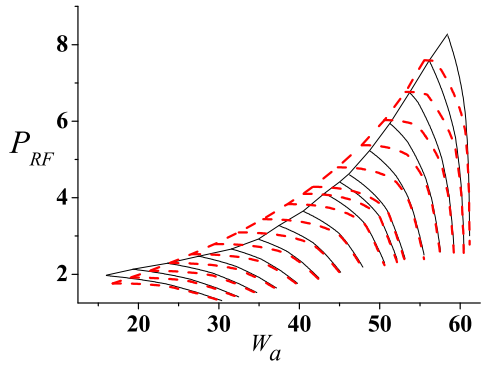

FIGURE 5. Comparison of fan component characteristics.

The different values ε correspond to different angle of guide vane. In order to illustrate the influence of guide vane angle on the engine performance, a relationship between ε and α is established.

$$\varepsilon = f(\alpha) \tag{5}$$

Different from the double bypass variable cycle engine with the core driving fan level (CDFS), the third stream is not mixed directly with the main flow. By adjusting the throat nozzle area of the third stream to match the mode selection valve, the third stream airflow and pressure could be controlled.

The open and close of mode selector valve directly determines the operation mode of the engine. The mode selection

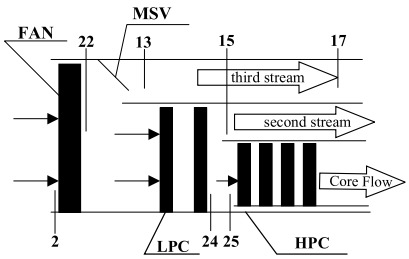

FIGURE 6. Simplified local structure of variable geometry turbofan.

valve, third duct and adjustable nozzle models are established below. Fig.6 shows the structure of the mode selection valve, third duct and the low-pressure compressor.

In the second bypass mode, the airflow of the fan tip enters into the third duct and the airflow of the blade root goes through the low-pressure compressor. In the single bypass mode, the blade tip and root airflow are mixed into the low-pressure compressor. Therefore, it is not suitable to establish the whole fan model. The fan needs to be split into fan blade root and tip model.

$$\begin{aligned} W_{a22t} &= W_{a2r}/(1 + X_{ht}) \\ W_{a22h} &= W_{a2r}X_{ht}/(1 + X_{ht}) \end{aligned} \tag{6}$$

where W_{a22h} and W_{a22t} is the conversion flow of fan blade tip and root. W_{a2r} is the conversion flow of the whole fan. X_{ht} is the fan airflow root/tip ratio.

The third stream airflow W_{g13} can be expressed as:

$$W_{g13} = W_{aft}(A_{MSV}/A_{13}) \tag{7}$$

where W_{aft} is the fan blade tip airflow, A_{13} is the maximum opening area of the third stream, A_{MSV} is the actual opening area of the mode selection valve.

When the engine is in the second bypass mode, the valve is completely opened ($A_{MSV} = A_{13}$) and the fan blade tip airflow goes through the third duct. When the engine is in double bypass mode, the valve is completely closed ($A_{MSV} = 0$) and no airflow flows into the third duct. The influence of valve on the airflow of the third duct could be calculated by the equation (7).

While adjusting the third stream airflow, the local pressure decreases as a result of the local drag, which is caused by the vortex and turbulence in the duct. In this paper, the process is considered as adiabatic. The local total pressure loss and the loss coefficient could be obtained from the [18].

$$\begin{aligned} \Delta p &= \zeta \frac{\rho V^2}{2} \\ \zeta &= 0.5(1 - \frac{A_a}{A_b}) \\ \sigma &= \Delta p/p_b \times 100\% \end{aligned} \tag{8}$$

where Δp is the change of local total pressure loss, ζ is the local loss coefficient, ρ is the air density, V is the section velocity, the subscript b and a are the section of the third stream nozzle area change, 'a' represents after,

'b' represents before. σ is the local total pressure loss coefficient, p_b is the section total pressure before the change.

The pressure loss of third duct can be calculated according to the formula (8). Through setting up the model of the total pressure loss, the tendency of its Mach number and total pressure loss coefficient are presented under different installed thrust, as shown in Fig.7.

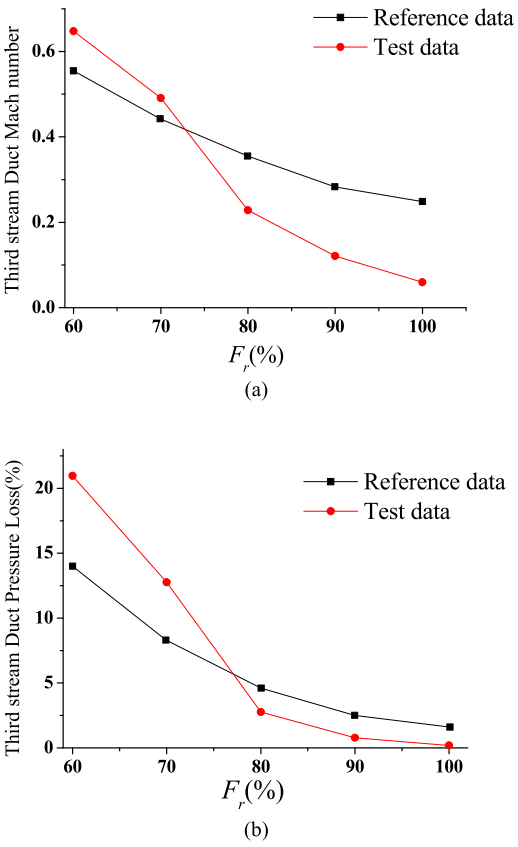

FIGURE 7. Fan duct Mach number & pressure drop.

As seen from Fig.7, the larger the installation thrust is, the less the total pressure loss would be. This also reduces the third stream duct Mach number. When the thrust of the third stream is small, the propulsion efficiency of the engine would decrease. All the airflow passes through the main duct and second stream duct, and only a small amount of airflow goes through the third stream duct. The calculation results of the above model are similar with the NASA [19], [20].

The inlet spillage drag is an increment of the outflow drag, which is relative to the design state. It is caused by the mismatching between the inlet's airflow supply and engine's airflow demand when the engine working state is changed. According to the general mixed pressure supersonic inlet flow spillage drag experience curve of AFRL (Air Force Research Laboratory) shown in Fig.8 and Fig.9, the inlet spillage drag could be calculated in the off-design condition.

The formula for calculating the inlet spillage drag could be expressed as,

$$F_{spill} = C_{d\ spill}(1/2\rho V_0^2)A_C \tag{9}$$

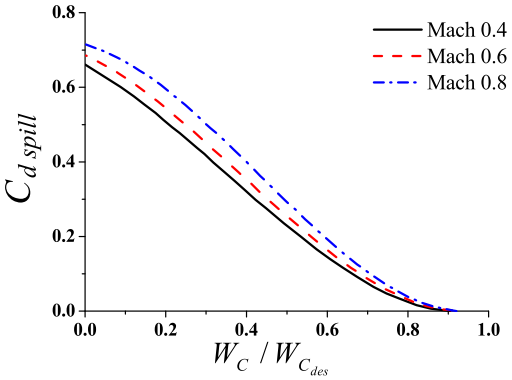

FIGURE 8. Fan duct Mach number & pressure drop.

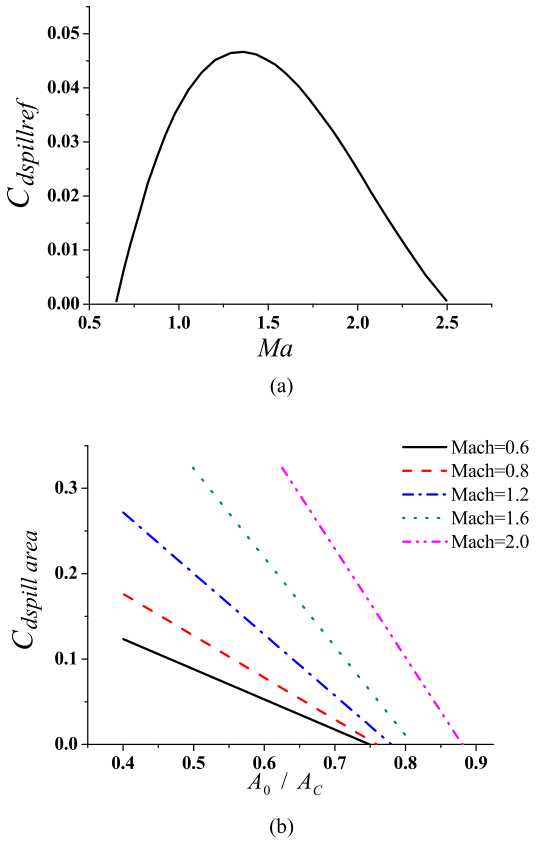

FIGURE 9. Supersonic spillage drag vs. airflow ratio.

where A_C is the inlet capture area, $C_{d\ spill}$ represents the spillage drag coefficient. During the supersonic flight, $C_{d\ spill}$ is the sum of $C_{d\ spill\ ref}$ and $C_{d\ spill\ area}$.

According to the above formula, the spillage drag could be obtained under all flight conditions if A_C is known. The inlet capture area can be calculated from the following formula.

$$\frac{W_{ain}}{A_0} = \frac{P_{std}}{T_{std}^{1/2}} M_0 (1 + 0.5(\gamma - 1)M_0^2)^{\frac{-(\gamma+1)}{2(\gamma-1)}} (\frac{\gamma g}{R})^{1/2} \tag{10}$$

where A_0 is the free flow area corresponding to the inlet airflow. P_{std} is the standard pressure at sea level. T_{std} is the standard temperature at sea level. W_{ain} is the inlet airflow.

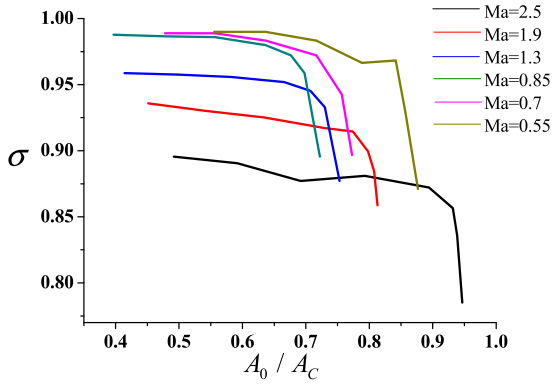

FIGURE 10. Throttling property diagram of inlet.

On the basis of inlet area A_0 and flow coefficient, the inlet capture area can be obtained. The inlet with certain geometrical characteristics has certain throttling characteristics. Fig.10 shows that the relationship between the total pressure recovery coefficient and the flow coefficient is given under the certain Mach number.

$$f(Ma, A_0/A_C, \sigma_{in}) = const \tag{11}$$

where *const* represents constant value.

When calculating the installation characteristics of the engine, not only the effect of internal airflow ought to be considered, namely the effect of the total pressure recovery coefficient on the dynamic and static engine performance, but also the effect of the inlet spillage drag on the installed thrust.

$$\begin{aligned} F_r &= F_n - F_{spill} \\ F_n &= F_n(U, \sigma) \\ T_{SFC} &= 3600 q_{mf}/F_r \end{aligned} \tag{12}$$

where F_n is the net thrust of the engine, F_r is the installed thrust, T_{SFC} is the installed specific fuel consumption, q_{mf} is the engine fuel flow, H is the altitude, Ma is Mach number, U is the engine control parameter.

$$U = [W_{fc}, \alpha_f, A_8, A_{18}, H, Ma]^T \tag{13}$$

where W_{fc} is the corrected fuel flow, α_f is the fan guide vane angle, A_8 is the throat area of the primary nozzle, A_{18} is the throat area of the third stream nozzle.

The modeling of combustion chamber, high and low pressure turbine, mixing chamber and exhaust nozzle will not go into details. The detailed modeling process can be referenced.

During the whole engine modeling, eight coupling equations are selected according to the flow continuity, static pressure balance and power balance.

$$E_i(U) = f_i(N) = 0 \tag{14}$$

where N is the initial guess value vector of the model, it can be expressed as,

$$\begin{aligned} N &= [n_1, n_2, n_3, n_4, n_5, n_6, n_7, n_8]^T \\ &= [n_l, n_h, X_{ht}, W_{g41C}, W_{g45C}, \pi_F, \pi_{LPC}, \pi_{HPC}]^T \end{aligned} \tag{15}$$

where n_l and n_h are the relative rotational speeds of the low and high pressure rotor, W_{g41c} and W_{g45c} are the conversion flows of high and low pressure turbine inlet, π_F is the pressure ratio of fan, π_{LPC} is the pressure ratio of low pressure compressor, π_{HPC} is the pressure ratio of high pressure compressor.

In this paper, the model takes the ground condition as the design point. The eight coupling equations contained by the steady model are shown as below.

1. Power balance residual function of high pressure rotor:

$$\varepsilon_1 = \frac{H_{pt}}{H_{pc} + H_{pext}} - 1 \tag{16}$$

where H_{pt} is the power of high pressure turbine, H_{pc} is the consumed power of low and high pressure compressor and H_{pext} is extracted power of high pressure shaft.

2. Power balance residual function of low pressure rotor:

$$\varepsilon_2 = \frac{H_{pl}}{H_{pf}} - 1 \tag{17}$$

where H_{pl} is the power of low pressure turbine, H_{pf} is the consumed power of fan.

3. Flow continuity residual function of high pressure turbine inlet:

$$\varepsilon_3 = \frac{W_{g41C,x} - W_{g41C}}{W_{g41C}} \tag{18}$$

where $W_{g41C,x}$ is the high pressure turbine initial guess flow and W_{g41C} is the calculated flow.

4. Flow continuity residual function of low pressure turbine inlet:

$$\varepsilon_4 = \frac{W_{g45C,x} - W_{g45C}}{W_{g45C}} \tag{19}$$

where $W_{g45C,x}$ is the high pressure turbine initial guess flow and W_{g45C} is the calculated flow.

5. Static pressure balance residual function of bypass outlet:

$$\varepsilon_5 = \frac{P_{S6}}{P_{S163}} - 1 \tag{20}$$

where P_{S6} is the internal static pressure at the outlet of bypass and P_{S163} is the external static pressure at the outlet of bypass.

6. Pressure balance residual function of nozzle throat:

$$\varepsilon_6 = \frac{P_{8c}}{P_8} - 1 \tag{21}$$

where P_{8C} is total pressure calculated by flow and P_8 is the total pressure calculated by inflow pressure.

7. Flow continuity residual of fan:

$$\varepsilon_7 = \frac{W_{a22h}}{W_{a24}} - 1 \tag{22}$$

where W_{a22h} is airflow of Fan blade root, W_{a24} is the airflow of low pressure compressor.

8. Pressure balance residual of fan:

$$\varepsilon_8 = \frac{P_{S22h}}{P_{S22t}} - 1 \tag{23}$$

where P_{S22h} is the static pressure of Fan blade root, P_{S22t} is the static pressure of Fan blade tip.

These equations can be solved by the Newton-Raphson method. Then the characteristic and performance parameters could be obtained.

The three ducts separate exhaust variable cycle engine has the characteristic of independent exhaust nozzle. By adjusting the fan guide vane angle, the area of third stream nozzle and primary nozzle, the engine actively control the bypass ratio and fan pressure ratio, which makes the engine have the constant flow characteristic. That is to say, the engine improves its installed performance, by keeping the flow constant to reduce the spillage drag in the throttling state. Therefore, the engine could match the airflow demand to the inlet's supply, aside from the regulation rules of the core engine speed that conventional engine needs to follow.

$$\begin{aligned} N_2 &= f_{W_{fc}}(W_{fc}) \\ W_{ain} &= W_{a2} = f_w(A_8, A_{18}, \alpha_f) = const \end{aligned} \tag{24}$$

The geometrical control quantities are monotonically related to the engine power state. The simulations are made to verify the effectiveness of open loop regulation. The formula (24) is further transformed as,

$$\begin{aligned} N_2 &= f_{W_{fc}}(W_{fc}) \\ A_8 &= A_{80} + k_1 f_{A_8}(W_{fc}) \\ A_{18} &= A_{180} - k_2 f_{A_{18}}(W_{fc}) \\ \alpha_f &= \alpha_{f0} - k_3 f_{\alpha_f}(W_{fc}) \end{aligned} \tag{25}$$

where the subscript 0 represents the corresponding value of crawling state, k1>0, k2>0, k3>0, $f_{A_8}(\bullet)$, $f_{A_{18}}(\bullet)$, $f_{\alpha_f}(\bullet)$ respectively represent the positive correlation coefficient and the function. The corresponding values in the envelope could be made into the form of interpolation table.

IV. NUMERICAL SIMULATION OF INSTALLATION PERFORMANCE

According to the open loop control law given by formula (25), the results of constant flow control have been verified.

The parameter changes and adjustment law of the engine are simulated in 10km and 0.8Ma, which are shown in Fig.11-13. The Figure 11 shows the control law of fan guide vane angle and the change of fan pressure ratio. With the increase of installed thrust, the fan guide blade angle decreases, which makes the speed of the fan decrease too. Keeping the inlet flow of the fan constant, the fan pressure ratio is on the rise.

The throat areas of third stream nozzle and primary nozzle are shown in Fig.12 and 13. With the increase of fuel flow, the primary nozzle area A_8 increases and then the area of third stream nozzle decreases, which makes the power of the low and high pressure turbine and inlet airflow increase. In order to keep the inlet airflow constant, it is necessary to reduce the area of third stream nozzle simultaneously. It makes the third stream airflow and fan's airflow decrease.

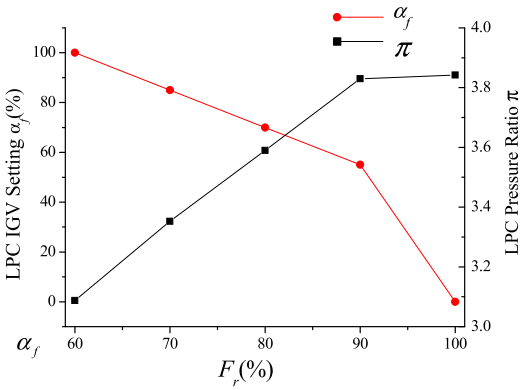

FIGURE 11. LPC pressure ratio changes (10km, 0.8 Ma).

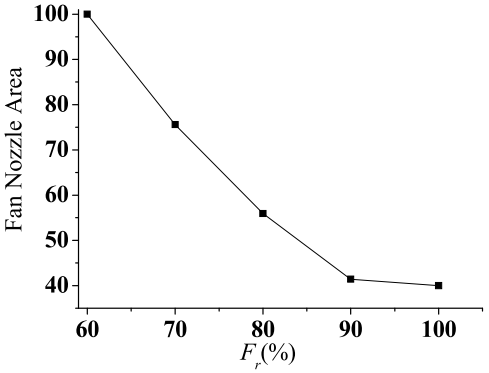

FIGURE 12. Fan nozzle throat area variations (10km, 0.8 Ma).

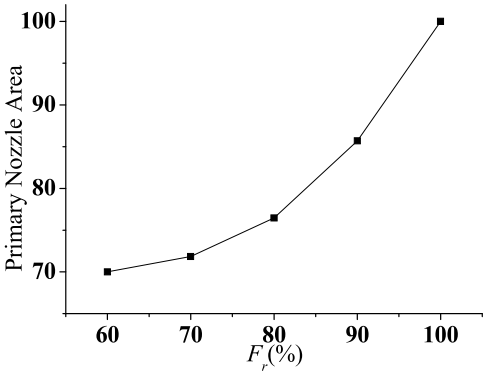

FIGURE 13. Primary nozzle throat area variations (10km, 0.8 Ma).

Fig.14 shows the relationship between the installed thrust and the flow change under the above constant flow control. With the increase of thrust, the pressure ratio of low pressure turbine and its power increase. Then W_{a25} and W_{g15} increase correspondingly. In order to keep the engine operation stable, the third stream nozzle area should be reduced, so that W_{g123} is decreasing. However, the engine whole airflow W_{a2} remains unchanged.

Fig.15(a) shows that the overall bypass ratio and B_{PR1} decrease. The second stream flow changes little with the installation thrust, which makes B_{PR2} basically unchanged.

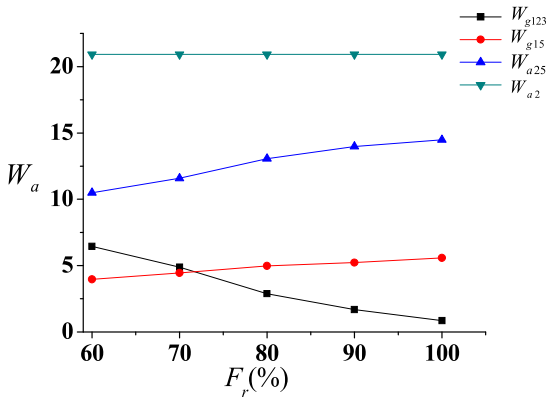

FIGURE 14. Internal airflow variations (10km, 0.8 Ma).

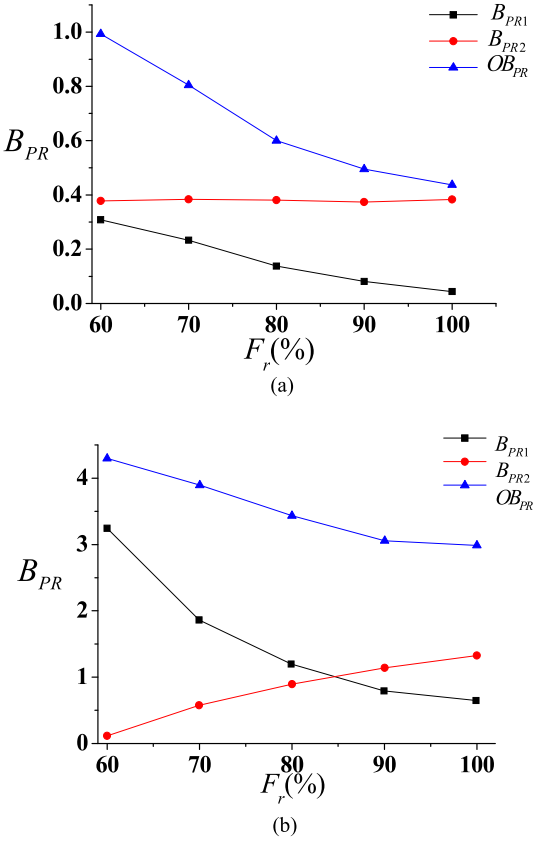

FIGURE 15. Bypass ratio changes (10km, 0.8 Ma).

The simulation results of reference are given in Fig.15 (b). It is proved by comparison that the variation trend of the flow is consistent under the same installation performance control law. And it further indicates that the model in this paper is certain credibility.

In the above control process, the engine needs to be guaranteed that its performance parameters (rotor speed, turbine inlet temperature) couldn't exceed limit and the engine wouldn't surge. As shown in table 1, the key parameters of the engine do not exceed the limit range when it is under constant flow control.

TABLE 1. Limits of engine parameter (H=10km, Ma=0.8).

Limit range	VALUE
$S_{Fan}\geqslant 10\%$	16.7%~40.6%
$S_{HPC}\geqslant 10\%$	18%~21.8%
$S_{LPC}\geqslant 10\%$	20.34%~22.4%
$N_l<105\%$	93.34%~104.42%
$N_h<105\%$	92.02%~101.98%
$N_f<105\%$	101.84%~105%
$T_{41}(K)<2000\ K$	1610K~1931.7K

During the typical supersonic cruise missions, the parameter changes and adjustment law of the engine are also simulated in 10km and 1.6Ma, which are shown in Fig.16 and Fig.17. Fig.16 shows the relationship between the installed thrust and the flow change. It can be seen that the change of each parameter is basically consistent with the subsonic state. And the changes of the bypass ratio in Fig.17 are also similar with the subsonic state.

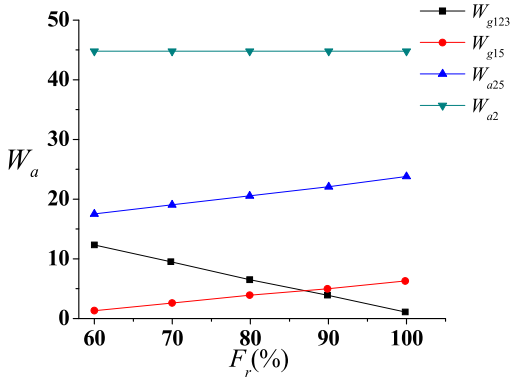

FIGURE 16. Internal airflow variations (10km, 1.6 Ma).

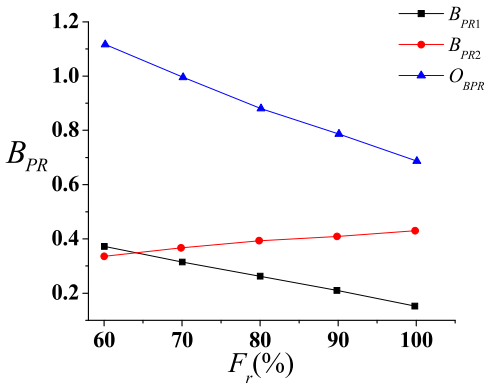

FIGURE 17. Bypass ratio changes (10km, 1.6 Ma).

The change of the key parameters of the engine is also given under this condition. As shown in Table 2, it can be

TABLE 2. Limits of engine parameter (H=10km, Ma=1.6).

Limit range	VALUE
$S_{Fan}\geqslant 10\%$	10.32%~51.74%
$S_{HPC}\geqslant 10\%$	23.8%~24.1%
$S_{LPC}\geqslant 10\%$	25.28%~32.02%
$N_l<105\%$	97.44%~102.65%
$N_h<105\%$	100.3%~104.69%
$N_l<105\%$	95.08%~95.74%
$T_{41}(K)<2000\ K$	1833.94K~1996.7K

seen that the performance parameters such as surge margin and rotational speed do not exceed the limit range.

Under the constant flow control, the trends of spillage drag and installed specific fuel consumption are further analyzed. In the subsonic typical operating point (H=10km, Ma=0.8), the change of the inlet spillage drag is shown in Fig.18.

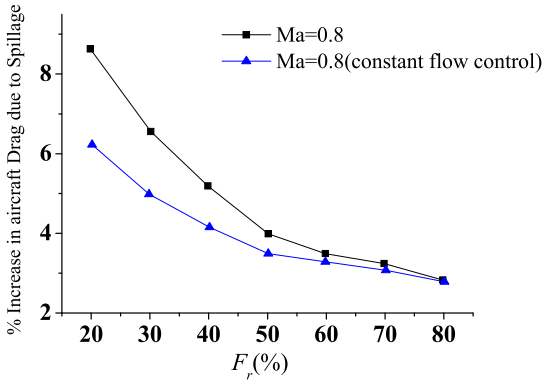

FIGURE 18. Subsonic cruise spillage drag.

As shown in the picture, the higher the installed thrust is, the less the spillage drag would be. The reason is that the engine's airflow demand increases, which makes the spillage airflow decrease. And there is no inlet shock wave drag at subsonic state, so the spillage drag coefficient would be small. When in the condition of deep throttling that the engine's airflow demand would greatly decrease, and then the inlet spillage drag would increase significantly. It can be seen in the picture that through the constant flow control, the inlet spillage drag can be reduced by about 2% in the throttling state.

Fig.19 shows the change law of thrust specific fuel consumption with installed thrust under subsonic cruise conditions. Because the bypass ratio increases, the thrust specific fuel consumption is reduced by about 2%~4% compared with the conventional turbofan engine.

In the supersonic cruise condition (H=10km, Ma=1.6), the change of inlet spillage drag is shown in Fig.20.

Under the constant flow control, the inlet spillage drag is reduced by about 9%. Owing to the increase of the spillage drag coefficient, the inlet spillage drag significantly increases. As shown in Fig.21, the thrust specific fuel

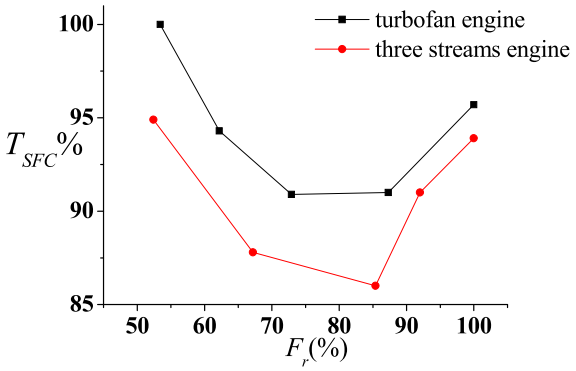

FIGURE 19. Thrust specific fuel consumption (10km, 0.8 Ma).

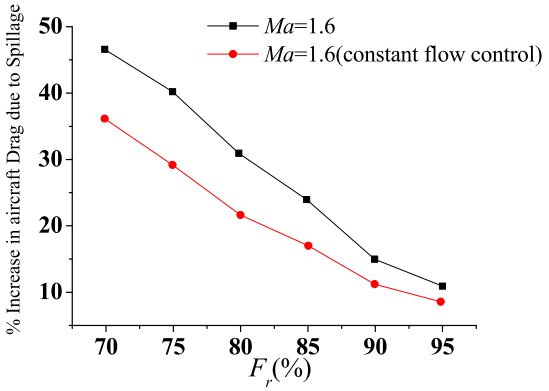

FIGURE 20. Supersonic cruise spillage drag.

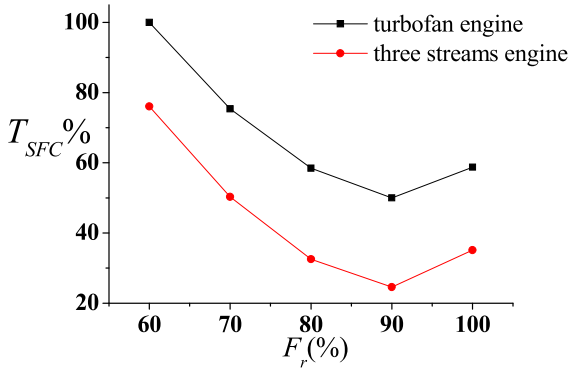

FIGURE 21. Thrust specific fuel consumption (10km,1.6 Ma).

consumption is 20% lower to the conventional turbofan engine. It indicates that the constant flow control can obviously improve the economy during the supersonic flight.

Fig.22 gives the engine speed characteristic simulation at the height of 10 kilometers, and also compares the constant airflow control scheme with the no constant airflow control. It shows that the constant flow control can significantly increase the installed thrust during the supersonic flight. So it is necessary to adopt the control to improve the installation performance of the engine.

Fig.23 shows the simulation comparison with the mixed flow three streams variable cycle engine . The whole

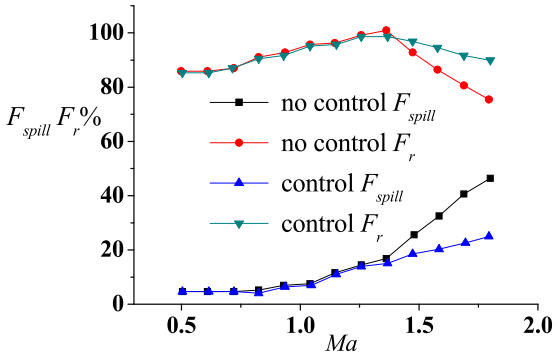

FIGURE 22. Comparison of F_{spill}, F_r.

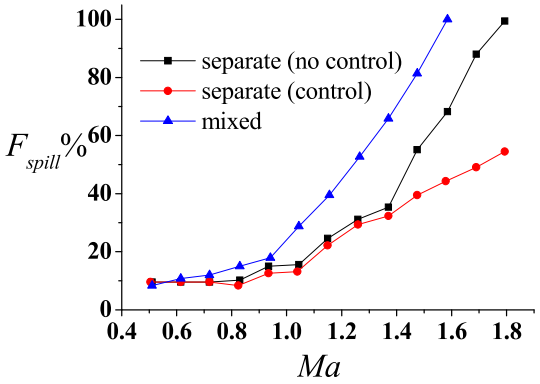

FIGURE 23. Simulation results of F_{spill}.

simulation is carried out at the height of 10 km and the engine is in the middle state. When the Mach number is larger than 1.5, by modulating the second and third streams, it is possible to match the engine's airflow demand to the inlet's airflow supply thereby reducing the spillage and increasing propulsive efficiency.

Compared with the mixed flow three streams variable cycle engine, the inlet spillage drag of the separate exhaust variable cycle engine is reduced by about 20%. The inlet spillage drag decreases more significantly under the constant flow control.

V. CONCLUSION

The three ducts separate exhaust variable cycle engine mathematical model has been established. Subsonic and supersonic cruise flight states (10km, 0.8*Ma* and 10km, 1.6*Ma*) were selected respectively to study the installation performance of the turbofan and variable cycle engine through simulation. Also the speed characteristics of engine (from 0.4*Ma* to 1.8*Ma*) at 10km were simulated. The following conclusions can be drawn.

(1) The model can accurately describe the influence of the engine states and performance parameters through the compression component guide vane, third stream nozzle and primary nozzle. Under the same installation performance control law, the change trend of the engine parameters is consistent with results of the NASA related research.

(2) It is possible to match the engine's airflow demand to the inlet's airflow supply through the certain variable geometric combination regulation. Compared with the mixed variable cycle engine, this engine effectively reduces the spillage drag and improves the installation performance of propulsion system. The inlet spillage drag is reduced by about 20%. Under supersonic flight condition, the constant flow control can obviously improve the economy of the engine.

In summary, the three ducts separate exhaust variable cycle engine mathematical model has been established and the control of inlet airflow which reduces the spillage drag is realized.

APPENDIX

NOMENCLATURE

Symbol	Explanation
MSV	Mode Selector Valve.
X_{ht}	Fan airflow root/tip ratio.
B_{PR1}	Bypass ratio 1.
B_{PR2}	Bypass ratio 2.
OB_{PR}	Overall bypass ratio.
LPC	Low pressure compressor.
HPC	High pressure compressor.
F_{spill}	spillage drag (N).
F_r	installed thrust(N).
C_{spill}	spillage drag coefficient.
S_{Fan}	Surge margin of Fan.
S_{LPC}	Surge margin of *LPC*.
S_{HPC}	Surge margin of *HPC*.
T_{SFC}	thrust specific fuel consumption.
ρ	Atmosphere density.
α	Vane guide angle.
R	Gas constant for air.

REFERENCES

[1] G. B. Bruening and W. S. Chang, "Cooled cooling air systems for turbine thermal management," *ASME Paper*, vol. 14, p. V003T01A002, 1999.

[2] G. Kopasakis, L. Cheng, and J. W. Connolly, "Stage-by-stage and parallel flow path compressor modeling for a variable cycle engine," in *Proc. AIAA/SAE/ASEE Joint Propuls. Conf.*, 2015, p. 4143.

[3] R. Brown, "Integration of a variable cycle engine concept in a supersonic cruise aircraft," in *Proc. Joint Propuls. Conf.*, 2011, p. 1049.

[4] E. Willis and A. Welliver, "Variable-cycle engines for supersonic cruising aircraft," in *Proc. 12th AIAA/SAE Joint Propuls. Conf.*, 1976, p. 759.

[5] Y. Lyu, H. Tang, and M. Chen, "A study on combined variable geometries regulation of adaptive cycle engine during throttling," *Appl. Sci.*, vol. 6, no. 12, p. 374, 2016.

[6] Z. Junchao, C. Min, and T. Hailong, "Matching mechanism analysis on an adaptive cycle engine," *Chin. J. Aeronaut.*, vol. 30, no. 2, pp. 706–718, 2017.

[7] X. Meng, Z.-L. Zhu, and M. Chen, "Steady-state performance comparison of two different adaptive cycle engine configurations," in *Proc. 53rd AIAA/SAE/ASEE Joint Propuls. Conf.*, 2017, p. 4791.

[8] N. K. Vallabhaneni. (2011). *Continuously Variable Rotorcraft Propulsion System*. [Online]. Available: https://www.lap-publishing.com/

[9] Y. Xu, M. Chen, and H. Tang, "Preliminary design analysis of core driven fan stage in adaptive cycle engine," in *Proc. AIAA/SAE/ASEE Joint Propuls. Conf.*, 2017, p. 4790.

[10] G. Xuezhong, Z. Wenxiang, and H. Jinquan, "Technology of Variable cycle engine component level modeling," *J. Aerosp. Power*, vol. 28, no. 1, pp. 104–111, 2013.

[11] J. S. Orme and T. R. Conners, "Supersonic flight test results of a performance seeking control algorithm on a NASA-15 spacecraft," in *Proc. AIAA Paper*, 1994, p. 3210.
[12] W. H. Ball and T. E. Hickcox, *Rapid Evaluation of Propulsion System Effects*, vol. 1. Seattle, WA, USA: Boeing Aerospace, 1978.
[13] Z. J. Wu *et al.*, "Research on genetic algorithm-based solution method for variable cycle engine model," *Appl. Mech. Mater.*, vol. 668, pp. 633–636, Oct. 2014.
[14] A. A. Sirinoglou, "Implementation of variable geometry for gas turbine performance simulation turbomatch improvement," M.S. thesis, Cranfield Univ., Cranfield, U.K., 1992.
[15] D. E. Muir, H. I. H. Saravanamuttoo, D. E. Muir, and D. J. Marshall, "Health monitoring of variable geometry gas turbines for the Canadian navy," in *Proc. Int. Gas Turbine Aeroengine Congr.*, 1988, pp. 244–250.
[16] J. Zheng, H. Tang, M. Chen, and F.-J. Yin, "Equilibrium running principle analysis on an adaptive cycle engine," *Appl. Thermal Eng.*, vol. 132, pp. 393–409, Mar. 2018.
[17] Z. Hong, W. Zhanxue, and L. Zengwen, "Impact of variable area bypass injector on variable cycle engine performance," *J. Aerosp. Power*, vol. 31, no. 12, pp. 2842–2850, 2016.
[18] J. Kurzke, "About simplification in gas turbine performance calculations," in *Proc. AMSE*, 2007, pp. 493–501, Paper GT2007-27620.
[19] J. W. Vdoviak, P. R. Knott, and J. J. Ebacker, "Aerodynamic/acoustic performance of YJ101/double bypass VCE with coannular plug nozzle," Gen. Electr. Company Aircraft Engine Bus. Group Cincinnati, Cincinnati, OH, USA, Tech. Rep. NASA CR-159869, 1981.
[20] R. J. Simmons, "Design and control of a variable geometry turbofan with an independently modulated third stream," *Diss. Abstr. Int.*, vols. 70–10, pp. 6369 and 124, 2009.

HAOYING CHEN is currently pursuing the Ph.D. degree with the College of Energy and Power Engineering, Nanjing University of Aeronautics and Astronautics. His major is aerospace propulsion theory and engineering. His research interests include modeling and model control of aero-engines.

HAIBO ZHANG received the Ph.D. degree from the Nanjing University of Aeronautics and Astronautics (NUAA) in 2005. He is a Professor with the College of Energy and Power Engineering, NUAA. His main research interests include modeling, fault diagnosis, vibration cancellation, and optimization control of aero-engines.

ZHONGZHI HU received the B.S. degree in automatic control from the Beijing Institute of Technology, China, and the M.S. and Ph.D. degrees in electrical engineering from The University of British Columbia, Canada.

He is a Professor with the Nanjing University of Aeronautics and Astronautics, Nanjing, China. As a researcher and an engineer, he has almost 30 years of extensive experience in modeling and simulation, controls and PHM for gas turbine, wind turbine, and other industry applications, including 15 years of R&D and engineering positions working for General Electric. He has published more than 40 refereed conference and journal papers, and holds five U.S. patents. His research interests are in gas turbine modeling, simulation, controls, and PHM.

QIANGANG ZHENG is currently pursuing the Ph.D. degree with the College of Energy and Power Engineering, Nanjing University of Aeronautics and Astronautics. His major is aerospace propulsion theory and engineering. His research interests include modeling, fault diagnosis, performance seeking control, and model predictive control of aero-engines.